Progress in Organic Coatings 117 (2018) 56–68

Contents lists available at ScienceDirect

Progress in Organic Coatings

journal homepage: www.elsevier.com/locate/porgcoat

Effect of tempera paint composition on their superficial physical properties-application of interferometric profilometry and hyperspectral imaging techniques

J.S. Pozo-Antonio[a,*], D. Barral[a], A. Herrera[b], K. Elert[b], T. Rivas[a], C. Cardell[b]

[a] Dpto. de Enxeñaría de Recursos Naturais e Medio Ambiente, Universidade de Enxeñaría de Minas e Enerxía, Universidade de Vigo, 36310, Vigo, Spain
[b] Dept. of Mineralogy and Petrology, Faculty of Science, University of Granada, 18071, Granada, Spain

ARTICLE INFO

Keywords:
Tempera paint mock-up
Interferometric profilometry
Hyperspectral imaging
Spectrophotometry
Reflectance

ABSTRACT

Interferometric profilometry and hyperspectral imaging techniques combined with traditional analytical techniques such as spectrophotometry, stereomicroscopy, X-ray diffraction, scanning electron microscopy, particle size analysis, and thermogravimetry were used to characterize tempera paint mock-ups. These paint mock-ups were prepared as binary mixtures made by mixing either egg yolk or rabbit glue binders with one of ten pigments traditionally used by mediaeval artists, namely lime, calcium sulfate, white lead, minium, hematite, cinnabar, azurite, lapis lazuli, blue smalt and malachite. We evaluated the effects of mineralogical composition, pigment particle size and morphology, as well as the type and concentration of the binder on the physical properties of the paintś surface. Results showed that all the above compositional aspects had a direct influence on the paintś color, reflectance, and roughness. Moreover, mineral impurities and neoformed minerals due to pigment-binder interaction during paint preparation had a crucial effect on the superficial physical properties of paints. The analytical results proved the usefulness of interferometric profilometry and hyperspectral imaging techniques for the characterization of paint surfaces. The gained information will help conservation specialists in the evaluation of the impact of conservation treatments on the paint surface and the assessment of surface damage caused by weathering processes.

1. Introduction

Over the last decades research has been conducted on historical paints and paint mock-ups to fully characterize their composition and weathering mechanisms when subjected to different aging scenarios [1–5]. The conformation of paints (i.e., the pigment's mineralogical composition and particle size, the type and content of binder, as well as pigment-binder interactions) not only determines their surface texture and color, but also their susceptibility to chemical and physical weathering [3,4,6–8]. Since color change is one of the most obvious consequences of the impact of adverse indoor/outdoor environments on paints, color spectrophotometry has been one of the preferred non-invasive techniques to evaluate alteration [4,5,9–12]. Often this technique has been combined with more invasive analytical techniques such as X-ray diffraction (XRD), scanning electron microscopy (SEM), Raman spectroscopy, and Fourier transform infrared spectroscopy (FTIR) to obtain more precise information on alteration processes involving compositional and conformational changes [3,6,13]. Many of these techniques require micro-sampling and are, thus, prohibitive in the case of valuable paintings.

More recently, non-invasive interferometric profilometry and hyperspectral imaging techniques have been introduced to the field of conservation science, providing useful additional information regarding superficial physical properties. The former allows high resolution measurements of surface roughness, and has been mainly applied for stone characterization [14]. Its application for the study of painting materials has been very limited [15]; recently Thei et al. [16] evaluated different consolidation treatments for urushi lacquer objects with this technique. Hyperspectral imaging techniques have been used for pigment identification [17,18], to evaluate the impact of conservation treatments [19], and to match paints for inpainting [20] based on their spectral features. However, until now the application of these imaging techniques has been often limited to case studies where only a small number of pigments/paints was analyzed [21,22].

Recently, a more general study using multispectral and hyperspectral imaging techniques was performed on paint [23]; however, this investigation did not consider pigment-binder interactions, pigment impurities, or particle morphology. Here we studied a wide range of

* Corresponding author.
E-mail address: ipozo@uvigo.es (J.S. Pozo-Antonio).

https://doi.org/10.1016/j.porgcoat.2018.01.007
Received 6 October 2017; Received in revised form 18 December 2017; Accepted 5 January 2018

pigments (i.e., lime, calcium sulfate, white lead, minium, hematite, cinnabar, azurite, lapis lazuli, blue smalt and malachite) in order to perform a systematic evaluation regarding the techniqueś potentials and limitations. The selected pigments were historically used in tempera paints for wall and panel paintings [24]. Mock-ups were prepared with pigments of different mineralogical composition, grain size and morphology using two different proteinaceous binders (i.e., rabbit glue and egg yolk) to evaluate the effect of pigment and binder properties as well as possible pigment-binder interactions on the paintś superficial physical properties (i.e, roughness, reflectance and color). To this end the above mentioned non-invasive techniques were combined with traditional analytical techniques, including spectrophotometry, stereomicroscopy, SEM, XRD, particle size analysis, and thermogravimetry (TG). The obtained results provided valuable information regarding shortcomings as well as potential applications of interferometric profilometry and hyperspectral imaging techniques for the characterization of painting materials and the evaluation of changes in the paintś superficial physical properties upon conservation treatments (e.g., impact of different cleaning methods) and physical and/or chemical weathering (e.g., assessment of changes during accelerated aging tests).

2. Materials and methods

2.1. Sample preparation

In this study we used forty-four tempera paint mock-ups prepared as binary mixtures mimicking real tempera paints. Each paint mock-up was prepared by mixing either egg yolk or rabbit glue with one of ten historic pigments (i.e. lime (calcite and/or portlandite), calcium sulfate (gypsum, bassanite and anhydrite), white lead, hematite, minium, cinnabar, azurite, lapis lazuli, blue smalt and malachite). Some pigments (i.e., lime, calcium sulfate, cinnabar, azurite and blue smalt) were purchased in different grain sizes in order to assess the effect of pigment particle size on the paint's superficial physical properties. All pigments were supplied by Kremer Pigments GmbH & Co. KG (Germany), except for cinnabar standard, which was supplied by Caremi Pigmentos S.L. (Spain). As mentioned before, the organic binders were of a proteinaceous nature; in particular, we used rabbit glue pearls (N°. 63028) from Kremer Pigments GmbH & Co. KG and egg yolk purchased locally.

Paint mock-ups were prepared according to Old Master recipes to achieve standards with adequate consistency similar to those used by mediaeval artists [25]. Consequently, these paints contained varying amounts of organic binder because binder demand depends on the pigmentś chemical composition and particle size; finer grained pigments commonly requiring more binder [24]. The procedure for the preparation of egg yolk-based paints can be consulted in [26], and for the rabbit glue-based paints in [6]. The paints obtained were applied in several layers onto glass slides (ca. 20 mm x15 mm x1 mm) using a paintbrush. The paint mock-ups were labeled by adding the letter E for egg yolk or G for rabbit glue to the pigments label, so as to clearly differentiate the powder pigments from the binary paint mixtures.

2.2. Analytical techniques

The pigments particle size was analyzed using a laser particle size analyzer (Mastersizer 2000LF, Malvern Instruments). Samples were dispersed in alcohol. One measurement was made per sample and the reported values are based on volume distribution.

The binder content of each tempera paint was determined by means of thermogravimetric analysis (TG) with a Shimadzu TGA-50H (Shimadzu Corporation) in flowing air (100 ml/min) at a constant heating rate of 10 °C min^{-1} (25–950 °C) as explained in [6,27].

Field emission scanning electron microscopy (FESEM) was used to study the pigmentśs morphological features (Auriga, Carl Zeiss, Germany). Equipment settings were 10^{-4} Pa vacuum and 3 kV beam accelerating voltage (secondary electron imaging mode). Samples were carbon coated.

The mineralogical composition of pigments and tempera paints was determined using X-ray diffraction (XRD, ẊPert PRO PANalytical B.V.) Analyses were performed using Cu-Kα radiation, Ni filter, 45 kV voltage, and 40 mA intensity. The exploration range was 3° to 60° 2θ and the goniometer speed was 0.05° 2θ s^{1}.The identification and semi-quantification (± 5%) of the minerals were carried out using Xpowder softare [28].

The viscosity of egg yolk- and rabbit glue-binder was measured using a Rheometer (R/S Rheometer, Brookfield Engineering Laboratories, Inc.) with a R/S MS-8 Din measuring system. Measurements were performed at 20 °C.

A stereomicroscope (SMZ 1000, Nikon) was used to examine the textural, structural and chromatic features of the paint mock-ups.

The color of tempera paints was characterized using CIELAB color space [29], measuring L* (lightness), a* and b* (color coordinates) and C^*_{ab} (chroma) by means of a Minolta CM-700d spectrophotometer. C^*_{ab} is calculated according to the following formula: $C^*_{ab} = (a^2 + b^2)^{1/2}$, where a* indicates the color position between red (positive values) and green (negative values) and b* between yellow (positive values) and blue (negative values). Fifteen random measurements on the entire surface of each mock-up (~20 × 15 mm) were obtained to provide statistically consistent results. The measurements were made in the Specular Component Included (SCI) mode, for a spot diameter of 3 mm, using D65 as the illuminant and an observer angle of 10°.

Reflectance spectra were obtained using an inhouse-built hyperspectral camera, which combines an imaging spectrograph with a monochrome matrix array sensor [30,31]. The equipment consisted of a CCD sensor Pulnix TM-1327 GE (1040 h x 1392 v pixel resolution) with an objective lens (10 mm focal length). An ImSpector V10 spectrograph with a spectral range of 400–1000 nm and a spectral resolution of 4.55 nm was positioned between the sensor and the lens. The camera scanned the surface, line by line, with a field of view of 51 × 0.89 mm, to obtain an image at each of the 1040 wavelengths. A cylindrical lens placed in front of the lamp focused the light so that the illuminated area was 15 × 1 cm. In order to move the sample, it was placed on a motorized XYZ translation stage in which the Z- axis is perpendicular to the sample surface. The paint mock-ups were fully scanned (ca. 20 × 15 mm). Once the hyperspectral images were acquired, the data were processed in a MATLAB programming environment in order to display the respective reflectance graphs.

Roughness was characterized by a non-contact optical profiling system using a profilometer (Wyko-NT 1100 (Veeco) with WycoVision®32 analytical software package). This equipment provides high resolution, 3D surface measurement, from sub-nanometer surface roughness to millimeter step-height. Two measurement modes are available: i) Phase-Shifting Interferometry (PSI) mode allowing high-resolution measurement of smooth surface and small steps, and ii) Vertical Scanning Interferometry (VSI) mode allowing the measure of rough surfaces and steps up to several millimeters high. In the current case, mean roughness data were obtained using the VSI mode (measurement range of 2 mm and vertical resolution of 1 nm for multi-measurement). The data were collected using a 5x magnification with an intermediate field of vision (FOV) lens of 1x. Using a motorized stage and the Data Stitching option, measurements were obtained of a 4 × 4 mm area by combining (stitching) 24 images. Reported values are based on one measurement.

The parameters computed for the characterizing of spatial and hybrid properties were Sa, Sdr and Str [32]. One measurement was made per sample. Sa is the height parameter in μm, measured over the complete 3D surface. Sdr is a hybrid parameter measuring the developed interfacial area ratio. It is expressed as the percentage of additional surface area contributed by the texture as compared to an ideal plane of the same size as the measured sample area. Str is the spatial parameter texture aspect ratio, which is a measure of the spatial

Table 1
Pigment properties and binder content of white tempera paints.

Pigment Properties							Paintś binder content	
Supplier pigment code	Supplier pigment size (μm)	Supplier pigment composition	Authorś pigment code	Authorś pigment size (μm)[a]	Authorś pigment composition[Φ] (wt.%)		Binder content in egg yolk- mock ups (wt.%)	Binder content in rabbit glue- mock ups (wt.%)
Calcite 58720	20	Calcite	CA-EF Calcite extra fine	25 0.25–100	Calcite Dolomite Quartz	90 10 Tr	11	8
Blanco San Giovanni 11415	120	Portlandite, Calcite	BSG-ST Calcite coarse	60 (5) 0.25–120	Portlandite Calcite	85 15	20	16
Blanco San Giovanni 11416	120 −1000	Portlandite, Calcite	BSG-C Calcite extra coarse	120 (2) 0.3–250	Portlandite Calcite	85 15	17	12
Gypsum alabaster plaster Italian 58340	< 75	Gypsum	G-EF Gypsum extra fine	7 0.2–85	Bassanite Anhydrite	65 35	13	18
Gypsum natural 58300 Selenite (Terra Alba)	80% < 20 18% < 25 1,9% < 32 1,9% < 32	Gypsum	G-F Gypsum fine	9 0.2 −75	Gypsum Anhydrite	35 65	8	10
Gypsum alabaster 58343	85% < 40	Bassanite	G-M Gypsum medium	16 1–160	Bassanite Anhydrite Dolomite	70 25 < 5	12	16
KREMER White 46000	< 45	Basic lead carbonate	WL White lead	3 0.1–10	Hydrocerussite Cerussite	50 50	23	16

[a] Main maximum particle size and particle size range. Numbers in parenthesis = secondary maximum particle size. Φ: Mineralogical composition (wt%) of pigments according to semi-quantitative (± 5%) XRD analysis. Calcite: $CaCO_3$; Portlandite: $Ca(OH)_2$; Gypsum: $CaSO_4{\cdot}2H_2O$; Bassanite: $CaSO_4.1/2H_2O$; Basic lead carbonate: $Pb(CO_3)_2{\cdot}Pb(OH)_2$; Dolomite: $CaMg(CO_3)_2$; Quartz: SiO_2; Anhydrite: $CaSO_4$; Hydrocerussite: $2PbCO_3{\cdot}Pb(OH)_2$; Cerussite: $PbCO_3$; Tr = trace.

isotropy or directionality of the surface texture. Str was calculated using a threshold value of 0.2 for the autocorrelation function.

3. Results and discussion

3.1. Pigment composition, binder demand and pigment-binder interaction of tempera paints

In order to perform a correct interpretation of the pigmentś superficial physical properties (i.e., roughness, reflectance and color), a detailed characterization of the pigmentś mineralogical composition and particle size, as well as the binder content and potential binder-pigment interactions is required. The results of this characterization are presented in three separate tables according to pigment color: white (Table 1), red (Table 2), and blue and green (Table 3). Each table contains the pigment specifications provided by the supplier, which are compared with our data on pigment mineralogy and particle size. Some general conclusions can be drawn from this comparison. The supplier did not always provide accurate information regarding the pigmentś mineralogical composition (i.e., natural gypsum (G-F) did not only contain gypsum, but also anhydrite, and G-M contained anhydrite additional to the bassanite stated by the supplier (Table 1)), and systematically omitted impurities such as quartz (i.e., detected in calcite, azurite, cinnabar, and hematite) and dolomite (i.e., detected in calcite, calcium sulfate, and hematite) (Tables 1–3). The detected impurities generally suggest a natural origin of the respective pigment (e.g., in natural deposits azurite is commonly associated with quartz and malachite and lapis lazuli typically contains calcite and diopside) and are not fillers deliberately added to reduce pigment cost [33]. These results evidenced the need of a detailed characterization of pigments prior to their use in conservation interventions or scientific studies. In the case of the later, the inclusion of pure synthetic equivalents might be necessary to determine the effect of impurities on pigment-binder interactions and the paintś superficial physical properties.

The supplierś particle size was unfortunately not reported in a systematic and precise manner (i.e., particle size was either reported as a range, average or as maximum particle size), even though almost all pigments were purchased from the same company. In some cases, the particle size reported by the supplier varied significantly from the values determined here, especially in the case of fine-grained pigments (e.g., white lead, minium, azurite standard, and malachite). Overall, it would be desirable to establish a standard methodology to report pigment particle size, including precise information on primary and secondary particle size maxima as well as the particle size range. Especially since it has been demonstrated that secondary maxima and particle size range can have an important effect on the paintś roughness (see section on Surface Roughness below). Note that in special cases (i.e., lime based-pigments, see Section 3.2) the data obtained from laser particle size analysis might be insufficient to evaluate paintś binder demand and accurately interpret data on superficial physical properties. Thus, additional microscopic analysis would be required to perform a more detailed pigment characterization.

Considering all paints included in this study, a direct relationship between binder demand and pigment particle size could not be established and the mineralogical composition was identified as the determining factor (i.e., relatively coarse blue smalt paints contained ~40 wt% egg yolk binder, whereas cinnabar paints prepared with pigments of similar size only contained 13–14 wt%). Apart from a few exceptions (i.e., calcium sulfate-based pigments), binder content was higher in paints prepared with egg yolk as compared with rabbit glue. This result can be explained with the much higher solid content of egg yolk (~50 wt%) as compared to rabbit glue (8 wt%) [34].

The majority of pigments studied here are insoluble in aqueous media [35] and mineralogical changes are not expected upon paint preparation. In some cases the formation of protein-metal complexes might occur, which could cause conformational changes in the proteinaceous binder but has no significant effect on the inorganic pigment [6]. Lime and calcium sulfate-based pigments, in contrast, undergo

Table 2
Pigment properties and binder content of red tempera paints.

Pigment Properties							Paintś binder content	
Supplier pigment code	Supplier pigment size (μm)	Supplier pigment composition	Authors' pigment code	Author's pigment size (μm)[b]	Author's pigment composition[Φ] (wt.%)		Binder content in egg yolk- mock ups (wt.%)	Binder content in rabbit glue- mock ups (wt.%)
Hematite 48651	1.5	Hematite	HE 0.6 (1.5) 0.3–17		Hematite Dolomite Quartz	Tr Tr	–	–
Minium 42500	< 63	Minium	MIN 3 (0.6) 0.4-9		Minium		~11	~10
Cinnabar[a] standard HGS PR 106	< 120	Cinnabar	CIN-ST Cinnabar standard 8 2–25		Cinnabar Quartz	Tr	17	11
Cinnabar very fine 10624	< 20	Cinnabar	CIN-EF Cinnabar extra fine 12 (0.6) 0.4–40		Cinnabar Quartz	Tr	23	11
Cinnabar medium 10627	50–63	Cinnabar	CIN-M Cinnabar medium 48 15–90		Cinnabar Quartz	Tr	14	13
Cinnabar dark, 10628	63–100	Cinnabar	CIN—C Cinnabar coarse 75 40–130		Cinnabar Quartz	Tr	13	12

[a] Pigment supplier is Caremi Pigmentos (Spain).
[b] main maximum particle size and particle size range. Numbers in parenthesis = secondary maximum particle size. −: Data not available. Φ: Mineralogical composition (wt%) of pigments according to semi-quantitative (± 5%) XRD analysis. Minium: Pb_3O_4; Hematite: Fe_2O_3; Dolomite: $CaMg(CO_3)_2$; Quartz: SiO_2; Cinnabar: HgS; Tr = trace.

partial dissolution and mineralogical changes, which influence the pigmentś binder demand as well as the paintś superficial physical properties. Lime-based pigments studied here (Table 1) included a natural ground calcite, which contained some typical impurities such as dolomite and quartz (CA-EF), as well as a standard and a coarse Bianco di San Giovanni (BSG-ST and BSG-C). The later pigments were prepared by a partial carbonation of calcium hydroxide (portlandite) [36]. According to XRD analysis both pigments contained ~85 wt% portlandite and ~15 wt% calcite and the mineralogical composition did not change significantly upon paint preparation [27]. In the case of lime-based pigments, the higher binder demand of BSG pigments as compared to the finer grained CA-EF is caused by the higher portlandite content in the former. Portlandite is significantly more hygroscopic than calcite and thus requires more binder [37]. Furthermore, FESEM imaging revealed that BSG-based pigments were constituted of nano-sized primary particles which formed larger aggregates (Fig. 1A). Upon mixing with an aqueous binder, these aggregates will partially disintegrate, resulting in a larger specific surface area and, consequently, higher binder demand [27]. A FESEM image for CA-EF pigment is included for comparison (Fig. 1B).

Table 3
Pigment properties and binder content of blue and green tempera paints.

Pigment Properties							Paint's binder content	
Supplier pigment code	Supplier pigment size (μm)	Supplier pigment composition	Author's pigment code	Author's pigment size (μm)[a]	Pigment composition according to authors[Φ] (wt. %)		Binder content in egg yolk- mock ups (wt.%)	Binder content in rabbit glue- mock ups (wt.%)
Azurite standard 10200 Deep greenish blue	< 120	Azurite	AZ-ST Azurite standard 22 0.2–55		Azurite Quartz Malachite	90 < 5 < 5	41	18
Azurite MP sky blue 10207 Light greenish blue	< 38	Azurite	AZ-EF Azurite extra fine 25 4–90		Azurite Quartz Malachite	70 20 > 5	24	11
Azurite MP Pale 10206, Light blue	38–63	Azurite	AZ-M Azurite medium 45 20-110		Azurite Quartz Malachite	85 10 5	33	12
Azurite MP Deep 10204, Dark blue	63–80	Azurite	AZ-C Azurite coarse 70 25-180		Azurite Quartz Malachite	85 10 5	24	10
Lapislazuli 10540, crystalline natural pale	< 80	Hauynite	LAP Lapis lazuli 47 0.6–95		Lazurite Calcite Diopside	> 80 ~20 Tr	27	18
Smalt very fine 10010	80 μm	Blue glass, Co-silicate	SM-C Smalt coarse 55 1–100		–		43[b]	21[b]
Smalt standard 10000	< 120 μm	Blue glass, Co-silicate	SM-EC Smalt extra coarse 75 1–140		–		37[b]	20[b]
Malachite	< 120 μm	Malachite	MAL 2–10 0.2–112[#]		Malachite Pseudomalachite Quartz	95 < 5 Tr	32	11

[a] Main maximum particle size and particle size range. Numbers in parenthesis = secondary maximum particle size. −: Data not available.
[b] Uncertain data. Φ: Mineralogical composition (wt%) of pigments according to semi-quantitative (± 5%) XRD analysis. Azurite: $Cu_3(CO_3)_2(OH)_2$; Quartz: SiO_2; Malachite: $Cu_2CO_3(OH)_2$; Hauynite: $(Si_3Al_3)Na_3CaO_{12}S$; Lazurite: $(Na,Ca)_8[(S,Cl,SO_4,OH)_2|(Al_6Si_6O_{24})]$; Calcite: $CaCO_3$; Diopside: $MgCaSi_2O_6$; Pseudomalachite: $Cu_5(PO_4)_2(OH)_4$; Tr = trace.

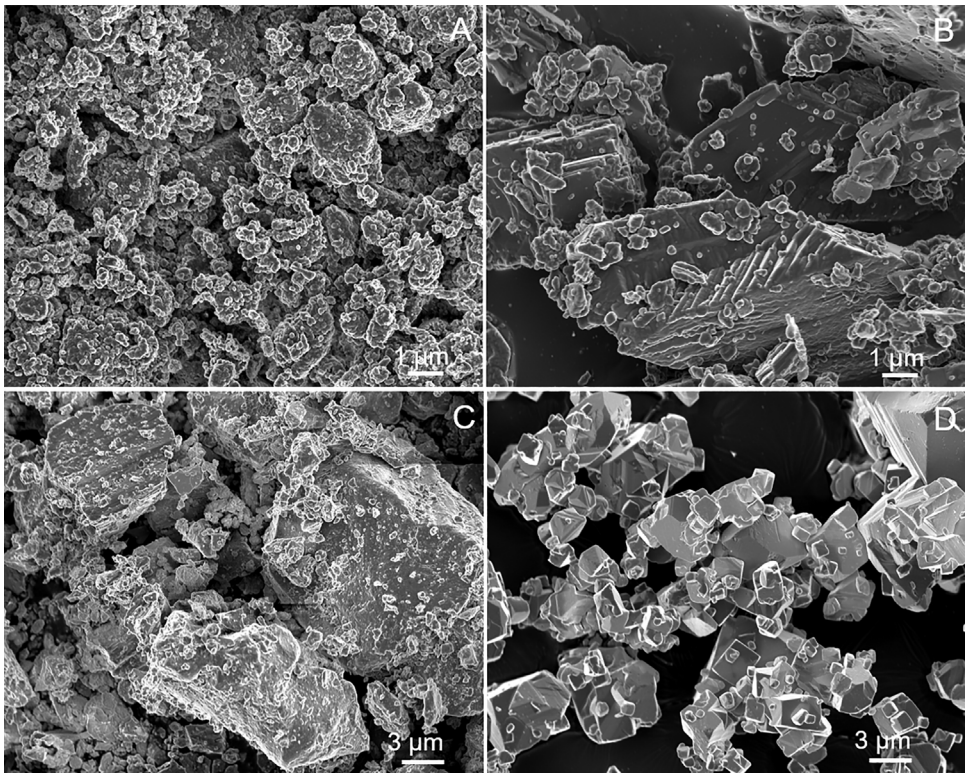

Fig 1. FESEM micrographs of pigments: (A) BSG-ST; (B) CA-EF; (C) CIN-EF and (D) CIN-ST.

Table 4
Mineralogical composition (wt%) of calcium sulfate-based pigments and paints according to semiquantitative XRD analysis.

Sample	Gypsum	Bassanite	Anhydrite	Dolomite
G-EF	–	65	35	–
G-EF-G	30	30	40	–
G-EF-E	–	55	45	–
G-F	45	–	55	–
G-F-G	40	–	60	–
G-F-E	35	–	65	–
G-M	–	70	25	< 5
G-M-G	–	60	35	< 5
G-M-E	–	50	45	< 5

Calcium sulfate-based pigments included G-F, a natural ground gypsum, as well as partially hydrated (G-M, containing a small amount of dolomite) and partially calcined (G-EF) gypsum (Table 1). These pigments commonly undergo phase changes due to hydration when mixed with an aqueous medium (i.e., anhydrite ($CaSO_4$) and bassanite ($CaSO_4{\cdot}1/2H_2O$) may transform partially or completely into gypsum ($CaSO_4{\cdot}2H_2O$) when in contact with water). However, the comparison of the mineralogical composition of calcium sulfate-based pigments and paints using semiquantitative XRD analysis (Table 4) revealed that pigments generally did not hydrate and in some cases (i.e., paints containing bassanite) actually underwent dehydration when mixed with either of the two binders. This is thought to be the result of the presence of organics, which, especially in the case of egg yolk, take up part of the water during paint preparation [34]. As a result, the hydration of anhydrite is hindered and the metastable bassanite actually dehydrates and partially transforms into anhydrite [38].

The lower binder demand of G-F as compared with G-M and G-EF is most likely related to compositional differences (i.e., it was the only calcium sulfate-based pigment which contained a large amount of gypsum). Our results suggest that binder demand will not only be influenced by the pigmeńts particle size, but rather be controlled by its chemical composition and physical properties (i.e., hygroscopicity), as well as pigment-binder interactions (i.e., dissolution and precipitation of new mineral phases).

3.2. Superficial physical properties of tempera paints

3.2.1. Stereomicroscopy

Stereomicroscopic observations revealed that tempera paints prepared with egg yolk generally had a slightly more yellowish tint than paints prepared with rabbit glue, which is explained by the relatively intense yellow color of the egg yolk binder as compared to rabbit glue (Figs. 2–4,). The color of red rabbit glue based-paints seemed more intense than the corresponding paints prepared with egg yolk (Fig. 3) and azurite paints with egg yolk seemed darker and more greenish than their rabbit glue counterparts (Fig. 4). Some green crystals (i.e., malachite according to XRD analysis) could be distinguished in coarse azurite paints (Fig. 4).

As expected, coarse pigments resulted in paints with a rougher surface than finer grained pigments. Brushstrokes, in contrast, were generally more evident in paints prepared with finer grained pigments (i.e., CA-EF, G-EF, G-M, WL, HE, CIN-EF and AZ-ST), especially when prepared with egg yolk binder. Brushstrokes were more evident in egg yolk-based paints because egg yolk had a much higher viscosity (476 ± 5 mPas) than rabbit glue (159.5 ± 3.6 mPas). Consequently, paints prepared with egg yolk had a much higher viscosity and, in many cases, were incapable of forming a homogeneous film. Furthermore, many paints prepared with fined grained pigments showed circular pockmarks on the paint's surface, which were relics of air bubbles. These pockmarks were especially pronounced in the case of egg-yolk-based paints prepared with extrafine calcite (CA-EF), calcium sulfate-based pigments (G-EF, G-F, G-M), white lead (WL), and malachite (MAL) (Figs. 2 and 4). A possible explanation for the formation of air bubbles is the presence of lecithin in egg yolk, which acts as a surfactant [39].

3.2.2. Color

Color measurements (Figs. 5–7) were generally in agreement with

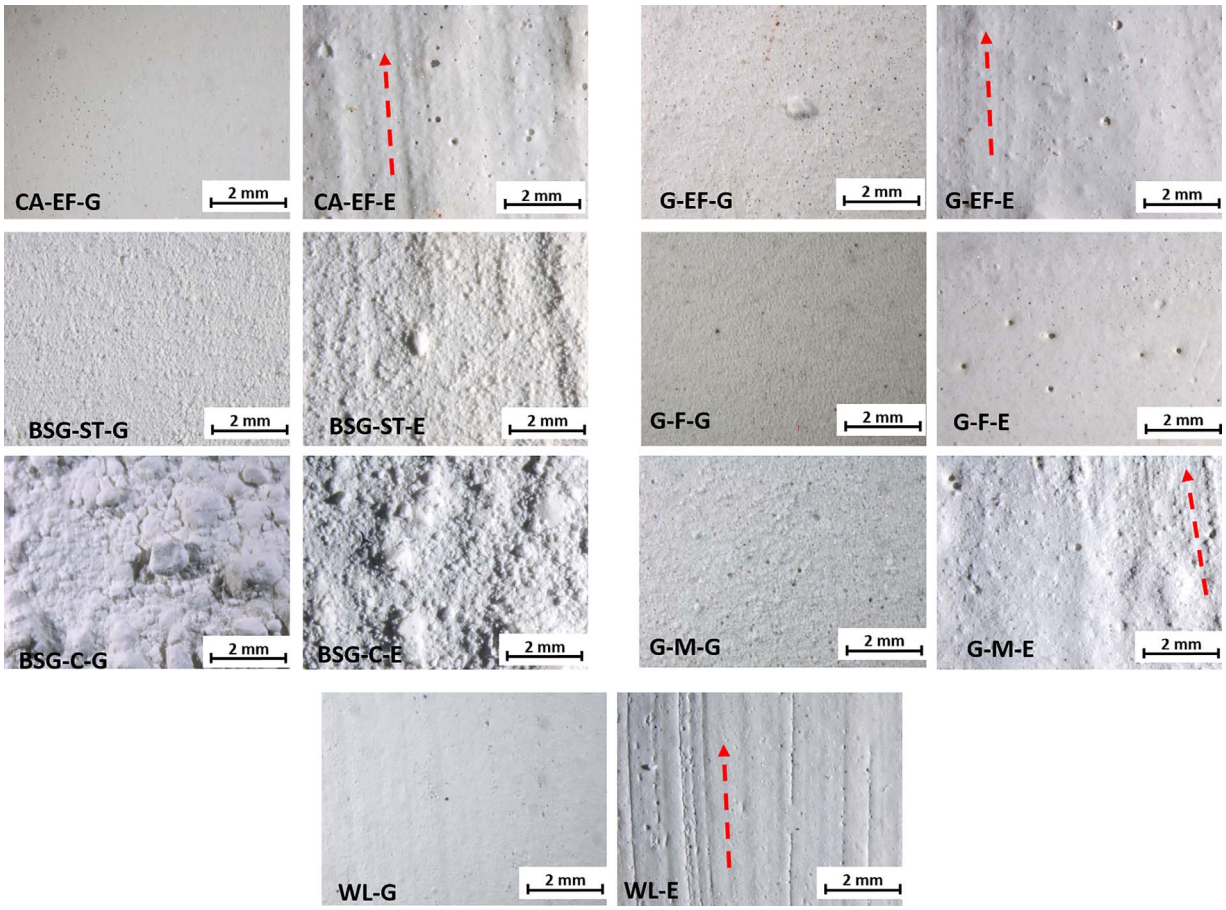

Fig. 2. Stereomicroscope micrographs of white tempera paints. See Table 1 for authors' paints code. Arrows indicate the direction of the brushstrokes.

stereomicroscopic observations. However, neither L* nor C^*_{ab} could clearly be related with the pigment particle size of white paints (Fig. 5). Note that we included color data with standard deviation for all paint mock-ups (see Table 1 in Supplementary Material). CA-EF showed a significantly lower L* as compared with the remaining lime-based paints, which was due to the substantial amount of dolomite in the former. Actually, color measurements showed that L* of CA-EF-based paints (containing ~10% dolomite) was 92.0, whereas L* of paints containing pure reagent grade $CaCO_3$ was 94.2 [27]. Overall the chemical composition of white pigments seemed to be the determining factor with respect to the measured color parameters. However, the paint color was influenced by the type of binder used for its preparation. It was found that C^*_{ab} values for egg yolk-based paints were generally much higher than for their rabbit glue counterparts. Certainly, the relatively strong yellowish color of the egg yolk binder was responsible for the observed increase in C^*_{ab}. No clear tendency regarding the influence of the binder type on L* could be detected.

A direct relation between L* and particle size could only be observed in paints prepared with cinnabar and rabbit glue (Fig. 6). Remarkably, L* decreased with decreasing particle size in these paints. As expected MIN-based paints had the highest L* and C^*_{ab} values, whereas HE-based paints showed the lowest C^*_{ab}. Generally, L* was higher in egg yolk-based red paints as compared to those prepared with rabbit glue. In these paints, it seemed that the binder did not influence the C^*_{ab} values significantly, because the yellow color of the egg yolk binder had only a very small effect of the overall color of red paints.

Color spectrophotometry revealed that contrary to cinnabar-based paints, fine grained azurite paints generally had a higher L* than coarser ones (Fig. 7). Differences in the chemical structure of both pigments are responsible for the observed phenomena. Whereas, covalent and ionic bonds are predominant in azurite, cinnabar has mainly covalent and metallic bonds (i.e., cinnabar being a semiconductor). Metallic bonds are responsible for the opacity (i.e., hiding power) of the later, which is related to strong absorbance at visible wavelengths (i.e., high values in the imaginary complex refractive index) [40]. Consequently, finely ground cinnabar showed lower specular reflection. Considering all blue paints, a clear relationship between particle size and L* was not observed and the mineralogical composition seemed to be the determining factor for the pigments color (i.e. conditioning their reflecting power). Generally, L* was significantly lower in blue paints prepared with egg yolk as compared with those prepared with rabbit glue. The egg-yolk binder also resulted in lower C^*_{ab} values, because paints turned more greenish.

It can be summarized that the binder effect on L* and C^*_{ab} depended on the original color of the pigment. Not surprisingly, upon mixing with the yellowish egg yolk binder, more important color changes were observed in white, blue, and green paints than in red paints. Particle size showed no clear relation with L* or C^*_{ab}. However, in the majority of paints a close relationship between L* and reflectance intensity could be established, in that paints with highest L* values had also highest reflectance.

3.2.3. Reflectance

White paints exhibited quite similar spectral features regardless of their chemical composition (Fig. 8). The main differences were observed between 400 and 500 nm, which however also depended on the type of binder used for paint preparation. Remarkably, BSG-pigments and WL mixed with egg yolk showed almost identical spectral features. This might be due to certain similarities in their chemical composition, considering that both pigments contain metal hydroxides and carbonates. The reflectance intensity could not always be related to the measured particle size. Note that in the case of BSG-pigments the size of

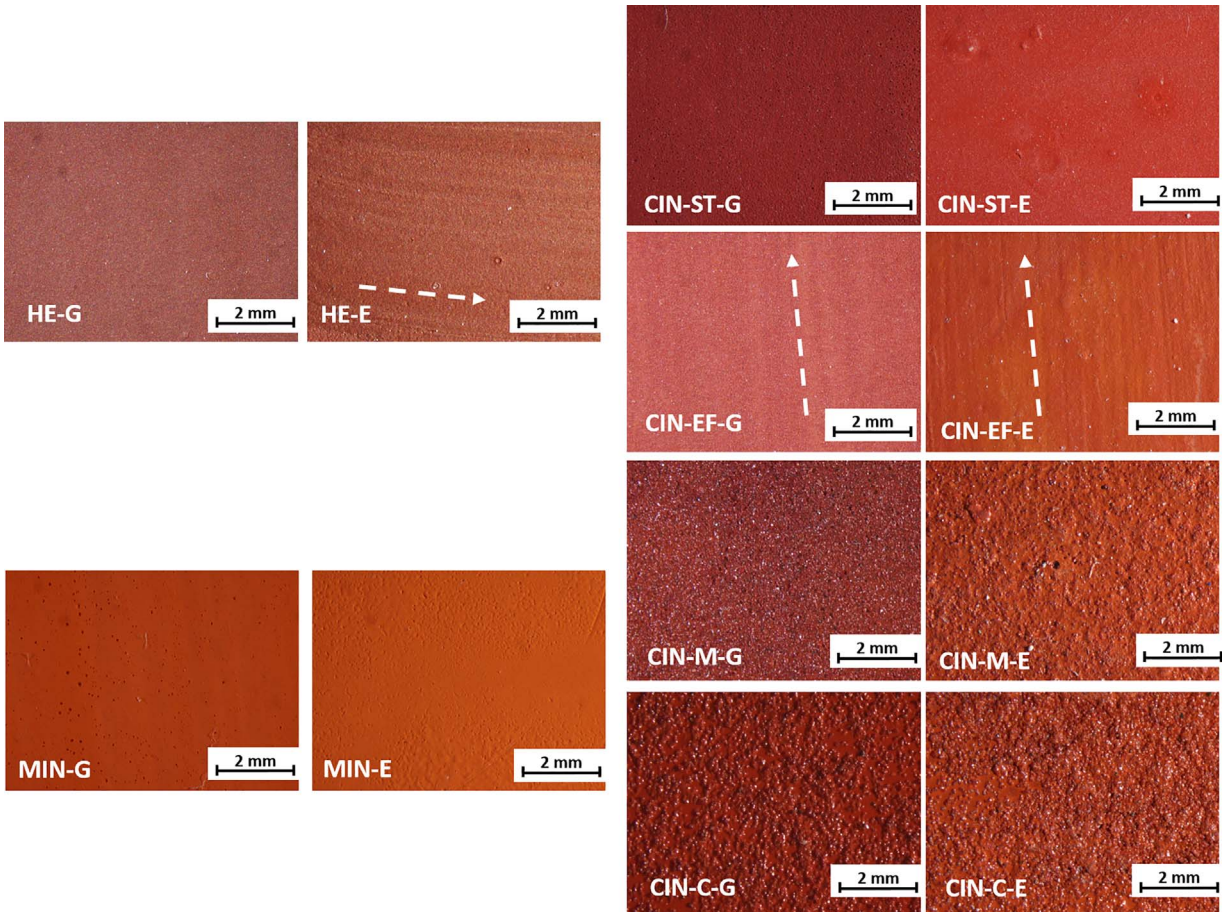

Fig. 3. Stereomicroscope micrographs of red tempera paints. See Table 2 for authors' paint code. Arrows indicate the direction of the brushstrokes (For interpretation of the references to colour in this figure legend, the reader is referred to the web version of this article).

primary nano-sized particles had to be considered, which were responsible for the higher reflectance observed in these paints (Fig. 8). The comparatively low reflectance of CA-EF pigments, independent of binder type, is thought to be caused by impurities detected in this pigment (i.e., 10 wt% dolomite and trace amounts of quartz [27]). Dolomite absorbs more light in the visible spectrum than calcite [41], thus reducing the total reflectance of CA-EF based paints. The trace amount of quartz (i.e., quartz having higher reflectance than calcite [42]) was insufficient to counteract this decrease. The significant difference in reflectance detected between G-F paints and paints prepared with either G-EF or G-M is also most likely caused by the presence of impurities in the case of the former. As mentioned previously, G-F is a ground natural gypsum, typically containing small amounts of carbonates and clays which determine the gypsuḿs color [43]. In our case the amount of impurities must have been relatively small (i.e. < 5 wt%) because they were not detected with XRD.

Reddish paints showed different spectral features over the visible spectrum, depending on their mineralogy (Fig. 9). The orange MIN-based paints had the highest reflectance intensity in the 550–675 nm range, whereas dark red HE-based paints showed the lowest reflectance intensity between 600 and 700 nm of all red paints, regardless of the binder type. Variations among CIN-based paints could be explained with differences in pigment morphology. CIN−C, CIN-M, and CIN-EF-based paints were prepared with pigments having irregular/fractured edges produced by the grinding of bigger lumps (Fig. 1C). Consequently, spectral features were very similar and their reflectance intensity could be related with the pigmentś particle size, especially in paints prepared with rabbit glue. CIN-ST-based paints, in contrast, contained particles with rhombohedral morphology as evidenced by FESEM (Fig. 1D). This morphology is characteristic for pigments obtained by a wet-process [44]. This fine grained pigment revealed slightly different spectral features and a much lower reflectance as compared with the remaining coarser CIN-based paints. These findings suggest that particle morphology has an important effect on the pigmentś reflectance properties. Furthermore, particle size measurements might not always be sufficient for an accurate interpretation of the pigmeńs superficial physical behavior and have to be combined with microscopic techniques to gain additional knowledge on particle morphology. Generally, the reflectance of red paints was slightly higher in egg yolk-based paints than in rabbit glue-based paints. Additionally, spectral features of egg yolk- and rabbit glue-based paints were almost identical.

Blue paints (Fig. 10) behaved similarly to red paints in that their spectral features and reflectance intensities were not only influenced by particle size, but also more importantly by the pigmeńs mineralogical composition. In fact, LAP-based paints (Fig. 10) were made up of medium-sized pigment particles but showed higher reflectance in the blue region (427–476 nm) than any of the other blue paints, independent of their pigment size. A direct relationship between particle size and reflectance was only observed among paints with identical composition (i.e., azurite based-paints), generally revealing higher reflectance as the particle size decreased. However, AZ-ST-based paints did not follow this trend, possibly as a result of the extremely high organic content (Table 3), which altered the paints reflectance properties. Actually, the spectrum of the AZ-ST-based paint mixed with rabbit glue was very similar to the ones of the remaining azurite-egg yolk paints. This is not surprising, because the pigment contained ~10.5% egg yolk, which had been added by the manufacturer [6].

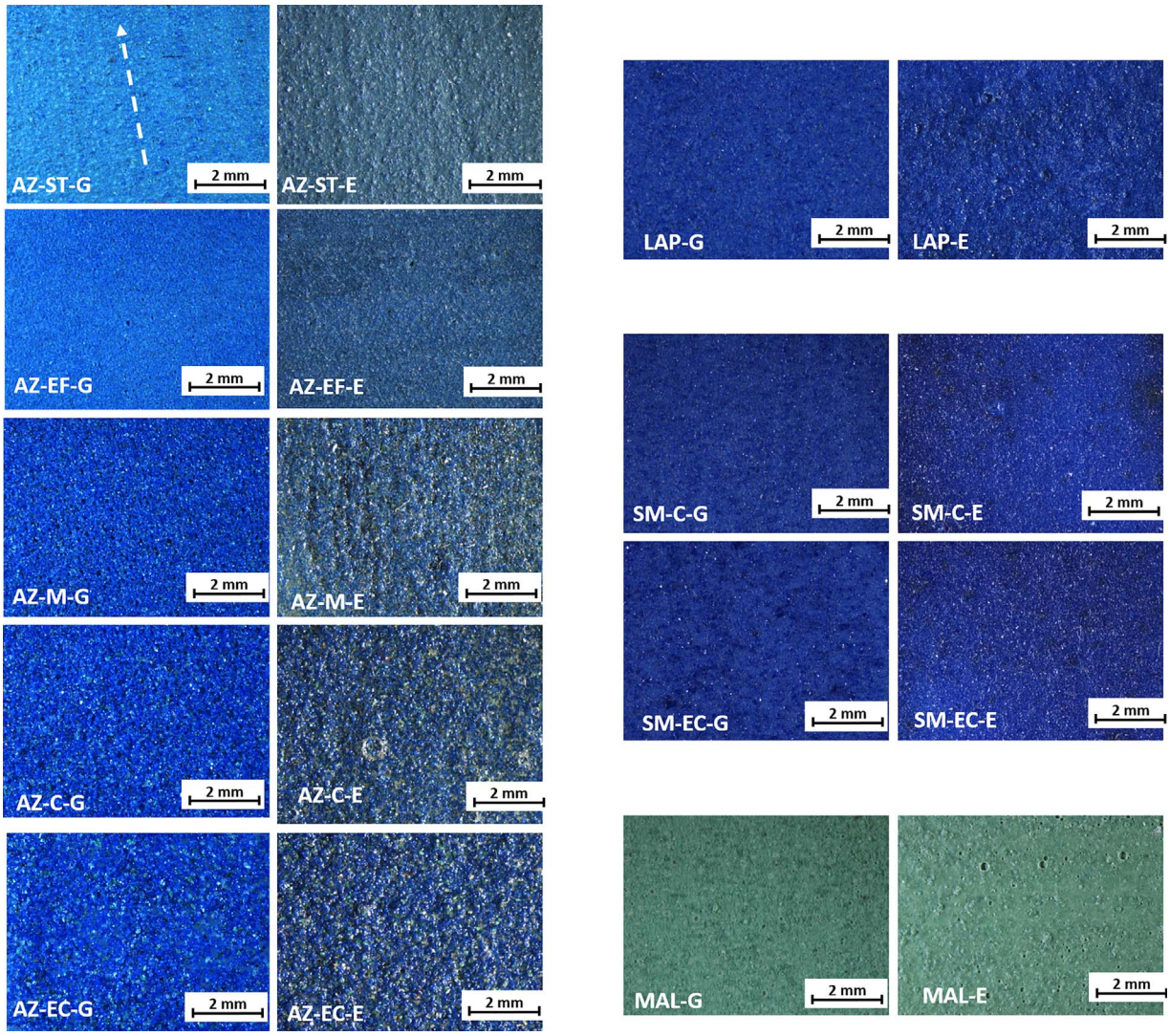

Fig. 4. Stereomicroscope micrographs of the blue and green tempera paints. See Table 3 for authors' paint code. Arrows indicate the direction of the brushstrokes (For interpretation of the references to colour in this figure legend, the reader is referred to the web version of this article).

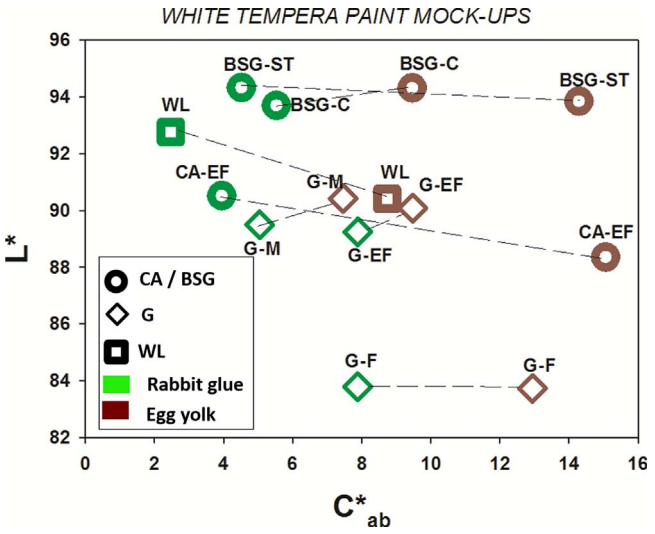

Fig. 5. L* and C^*_{ab} graph representing the color of the white tempera paints. See Table 1 for the authors' paint code. For interpretation of the references to color in this figure legend, the reader should refer to the web version of this article.

Liang et al. found a similar relationship between binder content and spectral reflectance in azurite paints mixed with different amounts of egg yolk [18]. In general, the reflectance spectra of blue and green paints showed distinct features depending on the binder type used for their preparation. Paints showed higher reflectance when prepared with rabbit glue as compared with egg yolk binder, especially in the case of the blue pigments. Possibly, egg yolk covered the pigment particle surface and acted as a filter. Yellow filters absorb preferentially radiation of higher energy in the blue region of the visible spectrum, thus, explaining the lower reflectance intensity of egg yolk-based paints [45]. Liang [23] observed a similar effect in the case of old yellowed varnish on blue paint.

Considering the results of all pigments, it was concluded that a direct relationship between particle size and reflectance power could only be established in paints prepared with pigments of identical composition (i.e., finer grained pigments resulted in higher reflection, [18,23]). Pigment composition seemed to be the most important parameter influencing reflectance properties. Impurities have to be considered because even small amounts of other minerals may cause significant changes in the paints reflectance as it was observed in the case of the lime-based pigments (CA-EF), which contained ~10 wt% dolomite. The possible formation of new mineral phases upon paint preparation should also be taken into consideration (i.e., formation of gypsum upon

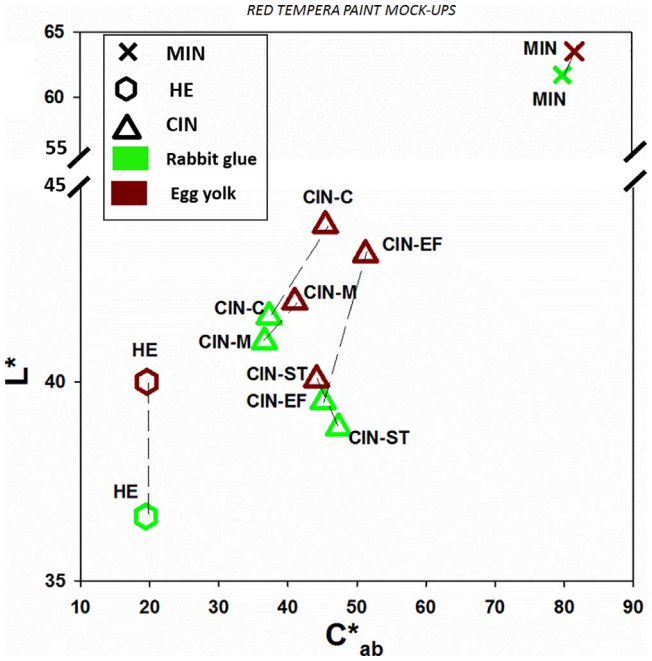

Fig. 6. L* and C^*_{ab} graph representing color values for the red tempera paints. See Table 2 for authors' paint code. For interpretation of the references to color in this figure legend, the reader should refer to the web version of this article.

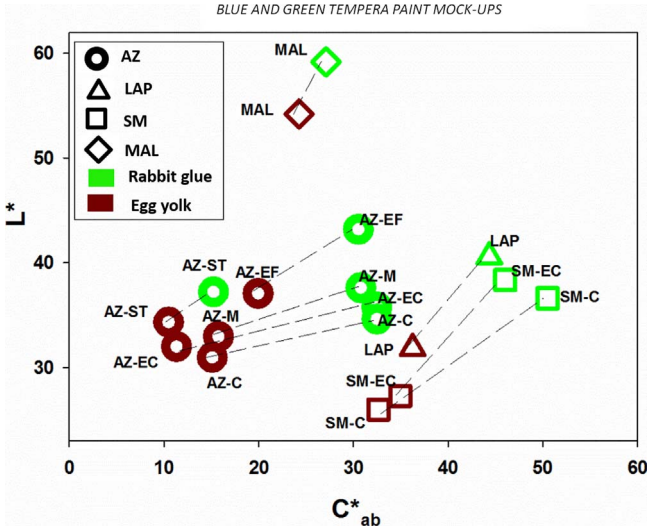

Fig. 7. L* and C^*_{ab} graph representing color values for the blue and green tempera paints. See Table 3 for authors' paint code. For interpretation of the references to color in this figure legend, the reader should refer to the web version of this article.

hydration of bassanite and anhydrite, or precipitation of calcite upon carbonation of portlandite). Moreover, particle morphology was also identified as a determining factor influencing reflectance. Analytical results suggest that reflectance measurements have only limited use for the identification of pigments, considering that white lead and lime-based paints prepared with rabbit glue showed almost identical spectra. Cosentino [46] also addressed the limited analytical capacity of this technique based on the study of 54 different pigments. The binder type influenced the paint́s spectral features. The data presented here showed that white, blue and green paints revealed different spectral features when mixed with either egg yolk or rabbit glue, whereas the reflectance of red paints seemed not greatly be influenced by the binder type. However, the identification of the binder type might not always be possible using hyperspectral imaging techniques alone, and a combination with traditional analytical techniques such as FTIR or gas chromatography might be required.

3.2.4. Surface roughness

As expected, the coarsest (CA-EC) and finest pigments (HE) produced paints with the highest and lowest Sa, respectively, independent of the type of binder used for their preparation (Fig. 11A). Generally, roughness increased with increasing particle size, following an exponential trend (Fig. 1A in Supplementary Material). The relationship between Sa and particle size was most evident in paints prepared with differently sized pigments of identical composition and similar binder content (i.e., azurite and cinnabar based-paints). Lime based-paints revealed large differences in Sa and BSG-ST mixed with rabbit glue showed a very low Sa. Possibly, amorphous calcium carbonate or small amounts of calcite (i.e., < 5 wt% which is the detection limit of XRD) formed during paint preparation and partially filled interparticle voids and led to a reduction in roughness [27].

With the exception of lime-based pigments, Sa generally showed also a direct relationship with the paint's binder content, independent of the binder type (Fig. 11A). When comparing two paints prepared with the same pigment, the one having the higher binder content always had a lower Sa because interparticle voids were filled more completely. It is important to highlight that brushstrokes contributed to surface roughness and, consequently influenced Sa, even though directionality is not considered in this parameter. A relatively small contribution of brushstrokes to overall roughness is evidenced in the case of white lead. White lead prepared with egg yolk had a higher Sa value than its rabbit glue-based counterpart, which contained less binder. This contradicts the general trend described above, indicating that paints with lower binder content generally had a higher Sa value. However, the higher Sa value can be explained with the presence of brushstrokes detected with optical microscopy in egg yolk-based white lead paints (Fig. 2), which contributed to the overall roughness.

In the case of Sdr (Fig. 11B, Fig. 1B in Supplementary Material), a clear relationship with the particle size was only observed in paints prepared with the same type of pigment and identical binder content (i.e., CIN-EF, CIN-M, and CIN-C mixed with rabbit glue). In these paints Sdr increased with increasing particle size. However, CIN-ST-based paint revealed a higher Sdr as compared to CIN-EF because of the different particle size distribution, even though, the former had a slightly smaller particle size and both paints were prepared with the same amount of binder (Table 2). Apparently, a larger number of relatively small particles in CIN-EF (i.e., CIN-EF has a main maximum particle size at 12 μm and a secondary maximum at 0.6 μm- (see Fig. 2 in Supplementary Material) partially filled interparticle voids and thus reduced Sdr (Fig. 11B). Note that small particles (< 1 μm) made up ~9 vol% of sample CIN-EF. Remarkably, paints prepared with coarse azurite pigments (AZ-EC, AZ-C, and AZ-M) generally had extremely high Sdr values. High Sdr values can be explained with the relatively narrow particle size range (see Fig. 1B and 2 in Supplementary Material) of these pigments, which were prepared using a special method for grain size separation [6], and the relatively low binder content of these paints in relation to their pigment particle size. As a result of the narrow particle size range, these paints hardly contained any small particles which could fill interparticle voids. The same applied for the low binder content, which did not fill voids and resulted in a paint surface of high spatial intricacy. Actually, the azurite paint prepared with AZ-M and egg yolk contained ~30% more binder than the remaining azurite/egg yolk-based paints. In this paint interparticle voids were filled more completely, resulting in a much lower Sdr. These results evidence the importance of a correct and detailed characterization of the pigmentś particle size distribution.

Considering Str, the obtained results revealed a clear relation between Str and the visibility of brushstrokes. Str values were highest in paints where brushstrokes were not observed, which was especially true for paints prepared with coarse pigments (i.e., pigment particle size > 25 μm), showing no directionality. With a few exceptions, paints

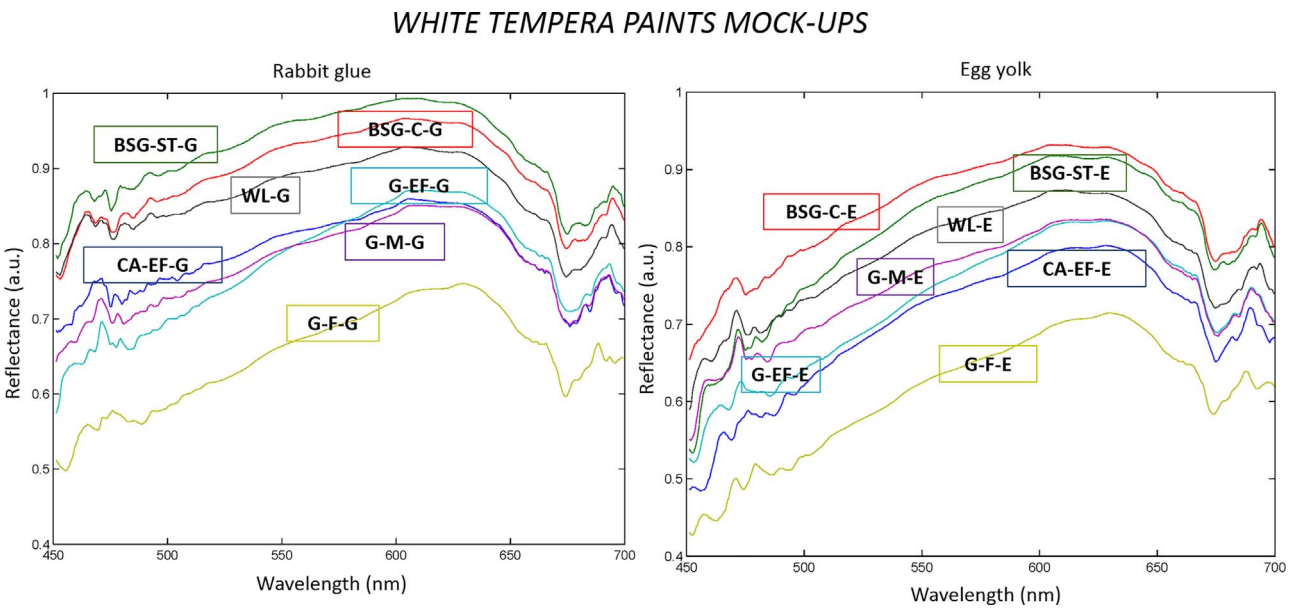

Fig. 8. Reflectance spectra of the white tempera paints with rabbit glue (G) and egg yolk (E) binder. See Table 1 for authors' paint code. For interpretation of the references to color in the ID boxes, the reader should refer to the web version of this article.

prepared with fine grained pigments and egg yolk binder (e.g., calcium sulfate-based pigments (G-F and G-M), white lead (WL), and hematite (HE)) had the lowest Str values (i.e., Str ≤ 0.1). This result was in general agreement with stereomicroscopic observation, revealing that these paints exhibited more evident brushstrokes. However, in some cases measured Str values were relatively high (i.e., ~ 0.4) even though the corresponding paints showed visible brushstrokes. It was concluded that the technique's ability to detect directionality decreases with increasing particle size and that a Str threshold at which brushstrokes were clearly visible could not be established (Fig. 1C in Supplementary Materials).

With respect to practical applications, Sa seems to allow an easier interpretation than Sdr. However, Sdr might provide important information regarding the paint́s susceptibility to weathering, which is greatly influenced by the specific surface area and its intricacy. Paints with larger surface areas and higher intricacy (indicated by a high Sdr value) will not only be more reactive and susceptible towards weathering but also allow for the deposition of a larger amount of particulate matter, which further contributes to the acceleration of weathering phenomena.

4. Conclusions

Based on the results of this study it was concluded that interferometric profilometry and hyperspectral imaging techniques can provide valuable information for the characterization of paints. Interferometric profilometry proved to be a sensitive tool for measuring surface roughness. This technique was able to detect very small differences in roughness caused by minor variations in the binder content or pigment particle size. Thus, it would be of particular value in comparative studies, for example to determine the cleaning method with the least impact on the surface characteristics of paints, to evaluate changes in roughness during weathering tests, or to estimate binder loss in paints. It might also be used to evaluate surface alteration of historic paints by

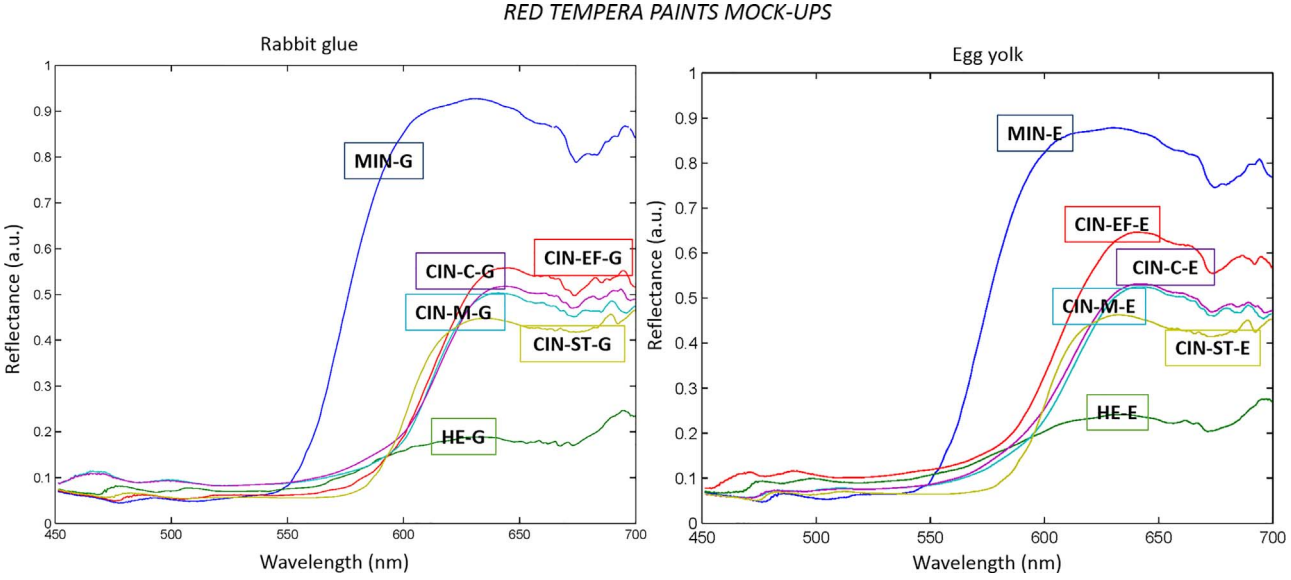

Fig. 9. Reflectance spectra of the red tempera paints with rabbit glue (G) and egg yolk (E) binder. See Table 2 for authors' paint code. For interpretation of the references to color in the ID boxes, the reader should refer to the web version of this article.

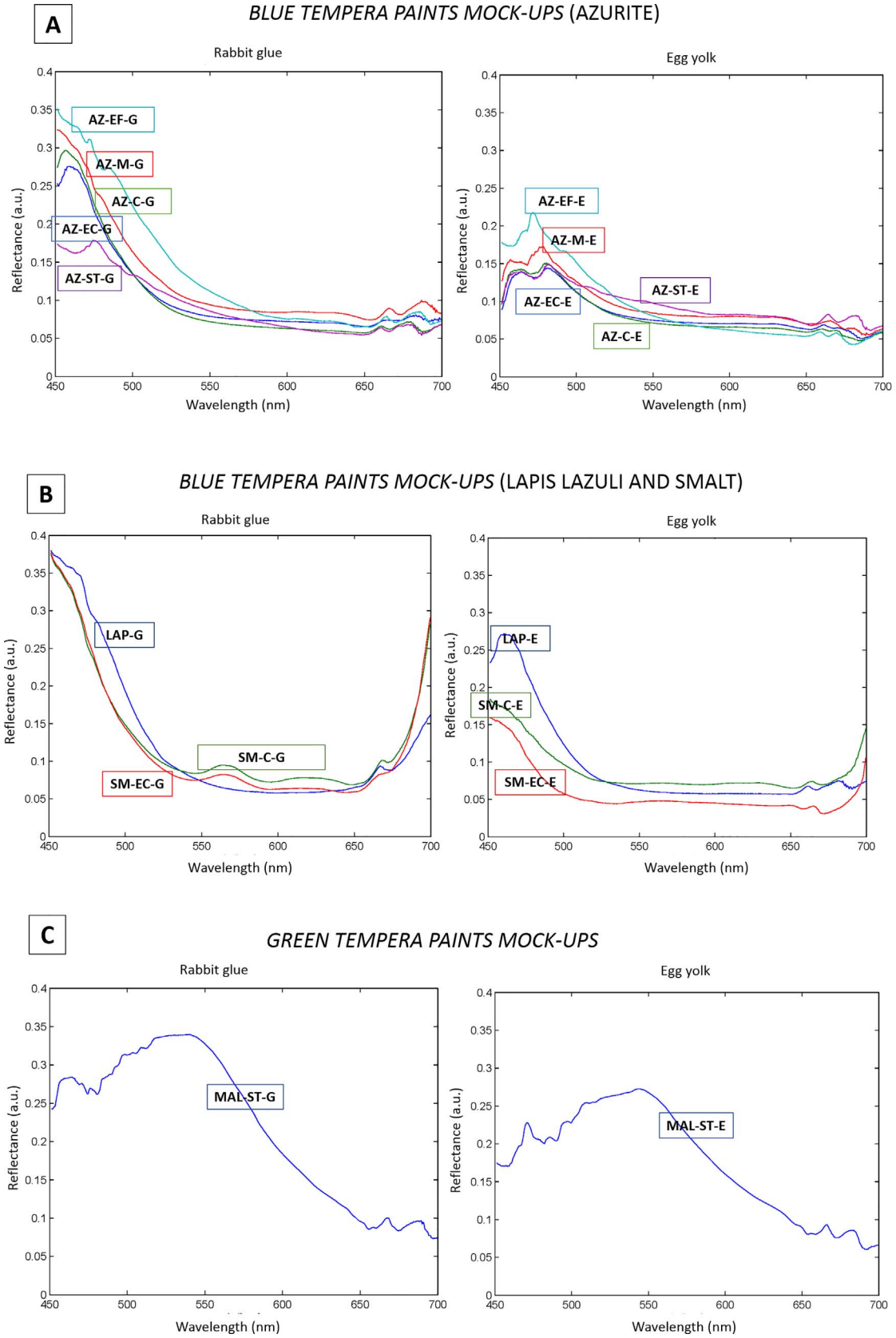

Fig. 10. Reflectance spectra for the blue (A, B) and green (C) tempera paints with rabbit glue (G) and egg yolk (E) binder. See Table 3 for authors' paint code. For interpretation of the references to color in the ID boxes, the reader should refer to the web version of this article.

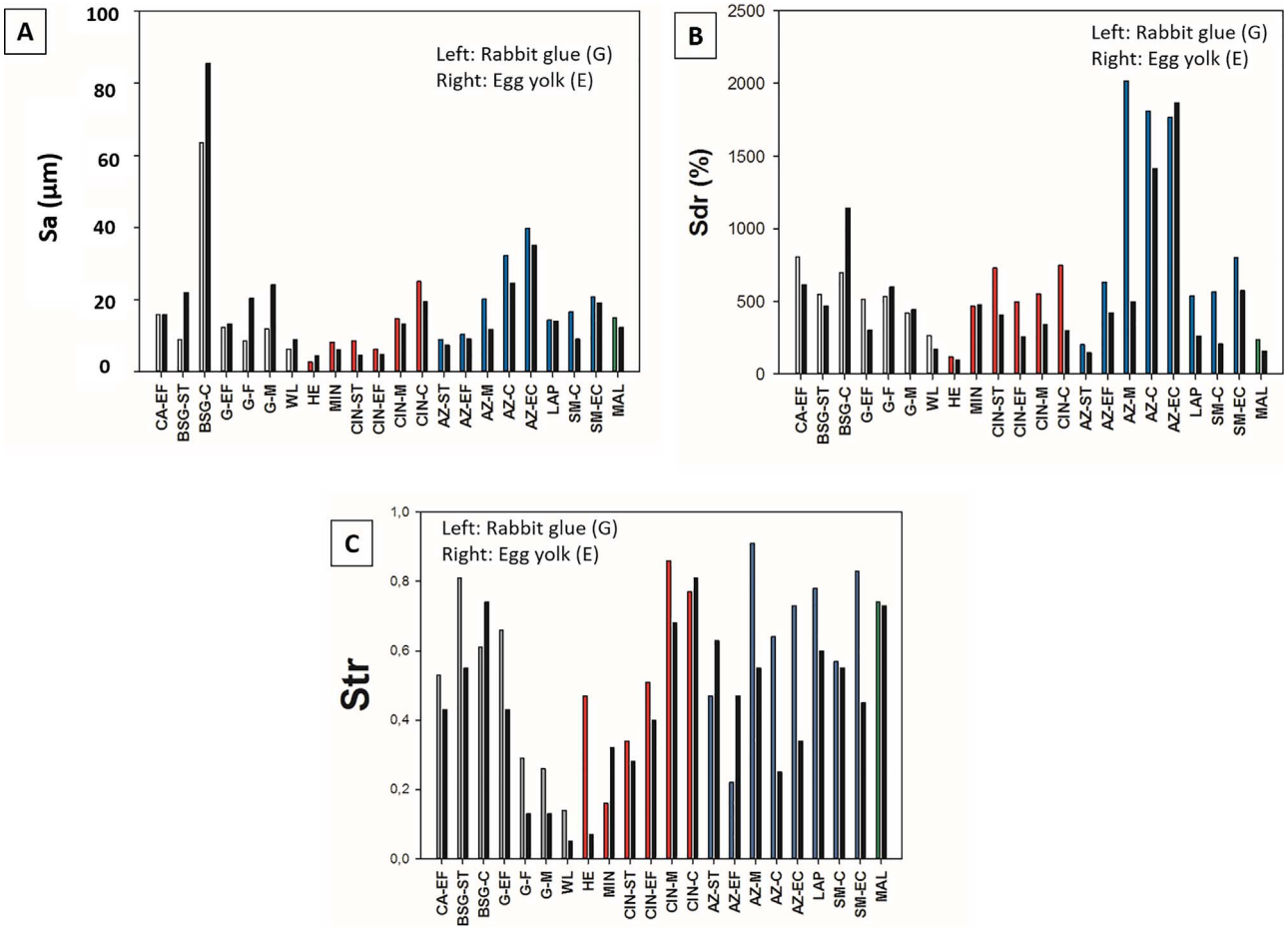

Fig. 11. Superficial roughness parameters for all paint mock-ups. A: Average roughness (Sa). B: Developed interfacial area ratio of the surface (Sdr). C: Texture aspect ratio (Str). See Tables 1–3 for the authors' paint code.

comparing spatial and hybrid parameters of different areas with identical color. In special cases a combination with SEM analysis might be advisable to determine the cause of the observed changes in roughness (e.g., binder loss, micro-pitting or crack formation). Furthermore, some discrepancies between roughness measurements and stereomicroscopic observations were detected. Considering the limited experience in the use of interferometric profilometry for roughness measurements of relatively inhomogeneous and complex paint surfaces, more research will be needed to determine the influence of surface morphology/inhomogeneity (e.g., effect of the presence of isolated inhomogeneities such as pockmarks) on spatial and hybrid parameters and establish the reliability of the obtained measurements.

Previous studies have identified a wide range of applications for hyperspectral imaging techniques in the field of conservation science. However, results obtained here revealed certain limitations of this technique with respect to the identification of pigments in simple binary paint systems, in that certain paints had very similar spectral features despite their different mineralogical composition that determines their different reflecting power. In general, the paińts spectral features were not only influenced by the pigmeńts composition, but also by the pigmeńts morphology and the type of binder used for its preparation. Furthermore, impurities, pigment particle size, and binder content had an important impact on reflectance intensity. These findings suggest the need for a comprehensive database of reference spectra considering all these variables.

Our analytical results further revealed that pigment composition was the most important parameter, directly or indirectly controlling the paińts color, reflectance, and binder demand; the later, in turn, having an important influence on surface roughness.

Unfortunately, suppliers' data on pigment composition might not always be reliable. Thus, an exhaustive identification of the pigment composition, impurities as well as possible compositional changes upon paint preparation has to be performed using traditional analytical techniques such as XRD, FTIR, or Raman spectroscopy in order to correctly interpret data on surface physical properties. Particle size was also recognized as an important factor, influencing the paińts binder demand, color, reflectance and surface roughness. Again, supplierś data proved to be incomplete or unreliable and a standardized methodology would be desirable to correctly characterize particle size. In special cases (e.g., lime-based pigments) laser diffraction might need to be combined with SEM to obtain more detailed information on the size of aggregated primary particles. SEM would also be a useful tool to accurately characterize pigment morphology, which has been identified as an important parameter influencing spectral features and reflectance intensity.

The binder type generally influenced spectral features of paints. The same is true for organics added during pigment preparation by the pigment manufacturer (i.e. AZ-ST). The binder content was identified as one of the controlling parameters of the paińts roughness and reflectance intensity. Thus, a detailed knowledge on binder type and content is mandatory to accurately interpret interferometric profilometry and hyperspectral imaging data. Overall it can be concluded that both techniques have to be combined with traditional techniques in order to perform a precise characterization of paints and paint alteration.

Acknowledgements

Financial support was provided by Spanish Research Projects AERIMPACT(CGL2012-30729) and EXPOAIR(P12-FQM-1889), the European Regional Development Fund (ERDF) and the Andalusian Research Group RNM-179. Analyses were performed in the CACTI Research Support Centre at the University of Vigo (Spain). J.S. Pozo-Antonio was supported by a postdoctoral contract with the University of Vigo within the framework of the 2011–2015 Galician Plan for Research, Innovation and Growth (Plan I2C) for 2014. J.A. Herrera was funded by a Spanish grant from the AERIMPACT Project (ref.BES-2013-065507). K. Elert is a post-doctoral researcher in the EXPOAIR Project. We thank the two anonymous referees for their insightful comments and suggestions.

Appendix A. Supplementary data

Supplementary data associated with this article can be found, in the online version, at https://doi.org/10.1016/j.porgcoat.2018.01.007.

References

[1] N.A. Katsanos, F. De Santis, A. Cordoba, F. Roubani-Kalantzopoulou, D. Pasella, Corrosive effects from the deposition of gaseous pollutants on surfaces of cultural and artistic value inside museums, J. Hazard. Mater. 64 (1999) 21–36.
[2] M. Odlyha, N.S. Cohen, G.M. Foster, Dosimetry of paintings: determination of the degree of chemical change in museum exposed test paintings (smalt tempera) by thermal analysis, Thermochim. Acta 365 (2000) 35–44.
[3] E. Manzano, J. Romero-Pastor, N. Navas, L.R. Rodríguez-Simón, C. Cardell, A study of the interaction between rabbit glue binder and blue copper pigment under UV radiation: a spectroscopic and PCA approach, Vib. Spectrosc. 53 (2010) 260–268.
[4] T. Rivas, J.S. Pozo-Antonio, D. Barral, J. Martínez, C. Cardell, Statistical analysis of color changes in tempera paints mock-ups exposed to urban and marine environment, Measurement (2017), http://dx.doi.org/10.1016/j.measurement.2017.06.037 (in press).
[5] A. Herrera, D. Ballabio, N. Navas, R. Todeschini, C. Cardell, Principal component analysis to interpret changes in chromatic parameters on paint dosimeters exposed long-term to urban air, Chemom. Intell. Lab. Syst. 167 (2017) 113–122.
[6] C. Cardell, A. Herrera, I. Guerra, N. Navas, L. Rodríguez Simón, K. Elert, Pigment-size effect on the physico-chemical behavior of azurite-tempera dosimeters upon natural and accelerated photo aging, Dyes Pigm. 141 (2017) 53–65.
[7] M. Price, A renaissance of color: particle separation and preparation of azurite for use in oil painting, Leonardo 33 (2000) 281–288.
[8] J. Romero Pastor, Interaction Between Historic Painting Materials, Benefit of Applying Spectrometric Techniques and Principal Component Analysis. PhD Dissertation, University of Granada, Spain, 2011.
[9] M. Bacci, M. Piccolo, S. Porcinai, B. Radicati, Tempera-painted dosimeters for environmental indoor monitoring: a spectroscopic and chemometric approach, Environ. Sci. Technol. 34 (2000) 2859–2865.
[10] M. Aceto, A. Agostino, G. Fenoglio, M. Gulmini, V. Bianco, E. Pellizzi, Non-invasive analysis of miniature paintings: proposal for an analytical protocol, Spectrochim. Acta A 91 (2012) 352–359.
[11] Z.C. Koren, Chromatographic and colorimetric characterizations of brominated indigoid dyeings, Dyes Pigm. 95 (2012) 491–501.
[12] M. Gil, T. Rosado, I. Ribeiro, J.A. Pestana, A.T. Caldeira, M.L. Carvalho, L. Dias, J. Mirão, A. Candeias, Are they fresco paintings? Technical and material study of Casas Pintadas of Vasco da Gama house in Évora (Southern Portugal), X-ray Spectrom. 44 (2015) 154–162.
[13] A. Durán, M.C. Jimenez de Haro, J.L. Perez-Rodriguez, M.L. Franquelo, L.K. Herrera, A. Justo, Determination of pigments and binders in pompeian wall paintings using synchrotron radiation – high-resolution x-ray powder diffraction and conventional spectroscopy – chromatography, Archaeometry 52 (2) (2010) 286–307.
[14] E. Doehne, C.A. Price, Stone Conservation–An Overview of Current Research, The Getty Conservation Institute, Los Angeles, 2010.
[15] B.G. Brunetti, M. Matteini, C. Miliani, L. Pezzati, D. Pinna, MOLAB a mobile laboratory for in Situ non-invasive studies in arts and archaeology, Vienna, 21–25.9.2005, in: LACONAVIJ, W. Nimmrichter, M. Kautek Schreiner (Eds.), Lasers in the Conservation of Artworks, 116 2018, pp. 453–456 (Springer Proc in Physics).
[16] J. Thei, S. Rivers, A.C. Taylor, A preliminary examination of urushi-based conservation options for the treatment of photodegraded Japanese lacquer using scanning electron microscopy and profilometry, Stud. Cons. 61S (2016) 131–148.
[17] M. Bacci, A. Casini, C. Cucci, A. Muzzi, S. Porcinai, A study on a set of drawings by Parmigianino: integration of art-historical analysis with imaging spectroscopy, J. Cult. Heritage 6 (2005) 329–336.
[18] H. Liang, K. Keita, B. Peric, T. Vajzovic, Pigment identification with optical coherence tomography and multispectral imaging, Proc. OSAV2008, 2nd Int. Topical Meeting on Optical Sensing and Artificial Vision, St. Petersburg, Russia, May 2008, 2018, pp. 33–42.
[19] W. Kautek, S. Pentzien, D. Müller-Hess, K. Troschke, R. Teule, Probing the limit of paper and parchment laser cleaning by multi-spectral imaging, SPIE Bellingham, in: R. Salimbeni (Ed.), Laser Techniques and Systems in Art Conservation, Proc. of SPIE, 4402 2001, pp. 130–138.
[20] R.S. Berns, J. Krueger M.Swicklik, Multiple pigment selection for inpainting using visible reflectance spectrophotometry, Stud. Conserv. 47 (2002) 46–61.
[21] A. Casini, F. Lotti, M. Picollo, L. Stefani, E. Buzzegoli, Image spectroscopy mapping technique for non-invasive analysis of paintings, Stud. Conserv. 44 (1999) 39–48.
[22] S. Baronti, A. Casini, F. Lotti, S. Porcinai, Multispectral imaging system for the mapping of pigments in works of art by use of principal-component analysis, Appl. Opt. 37 (1998) 1299–1309.
[23] H. Liang, Advances in multispectral and hyperspectral imaging for archaeology and art conservation, Appl. Phys. A 106 (2012) 309–323.
[24] H. Kühn, Erhaltung und Pflege von Kunstwerken und Antiquitäten 1, Keysersche Verlagsbuchhandlung., München, 1981.
[25] F. Pacheco, El arte de la pintura, Cátedra, Madrid, Spain, 1990.
[26] A. Herrera, N. Navas, C. Cardell, An evaluation of the impact of urban air pollution on paint dosimeters by tracking changes in the lipid MALDI-TOF mass spectra profile, Talanta 155 (2016) 53–61.
[27] K. Elert, A. Herrera, C. Cardell, Pigment-binder interactions in calcium-based tempera paints, Dyes Pigm. 148 (2018) 236–248.
[28] J.D. Martín-Ramos, Using XPowder A Software Package for Powder X-Ray Diffraction Analysis, (2004) GR 1001/04. ISBN 84–609-1497–6..
[29] Colorimetry Part 4: CIE 1976 L*a*b* Color Space, Commission Internationale De l'eclairage, CIE Central Bureau, Vienna, 2007 CIE S014–4/E: 2007.
[30] J.S. Pozo-Antonio, M.P. Fiorucci, A. Ramil, A.J. López-Díaz, T. Rivas, Evaluation of the effectiveness of laser crust removal on granites by means of hyperspectral imaging techniques, Appl. Surf. Sci. 347 (2015) 832–838.
[31] J.S. Pozo-Antonio, M.P. Fiorucci, T. Rivas, A.J. López, A. Ramil, D. Barral, Suitability of hyperspectral imaging technique to evaluate the effectiveness of the cleaning of a crustose lichen developed on granite, Appl. Phys. A. 122 (2016) 1–9.
[32] Geometrical Product Specifications (GPS)–Surface Texture: Areal– Part 2: Terms, Definitions and Surface Texture Parameters, (2013) (UNE-EN ISO 25178–2:2013. ISO 25178–2:2012).
[33] M. Pérez, K. Castro, M.D. Rodríguez, M.A. Olazabal, J.M. Madariaga, A critical analysis of commercial pigments, Proc. ART 2002, 7th Inter. Confer. on Non-destructive Testing and Microanalysis for the Diagnostics and Conservation of the Cultural and Environmental Heritage, University of Antwerp, Belgium,A ntwerp-Wilrijk, 2002, pp. 173–182.
[34] E.C.Y. Li-Chan, W.D. Powrie, S. Nakai, Chapter 6. The chemistry of eggs and egg products, in: W.J. Stadelman, O.J. Cotterill (Eds.), Egg Science and Technology, Food Products Press, New York, 1995, pp. 105–176.
[35] R.C. Weast, CRC Handbook of Chemistry and Physics, 59th ed. CRC Press, Boca Raton, FL, 1978-1979.
[36] E. Denninger, What is Bianco di San Giovanni of Cennino Cennini? Stud. Conserv. 19 (1974) 185–187.
[37] D.T. Beruto, F. Barberis, R. Botter, Calcium carbonate binding mechanisms in the setting of calcium and calcium-magnesium putty limes, J. Cult. Heritage 6 (2005) 253–260.
[38] A.E. Charola, J. Pühringer, M. Steiger Gypsum, A review of its role in the deterioration of building materials, Environ. Geol. 52 (2007) 207–220.
[39] B. Ozturk, S. Argin, M. Ozilgen, D.J. McClements, Formation and stabilization of nanoemulsion-based vitamin E delivery systems using natural surfactants: quillaja saponin and lecithin, J. Food Eng. 142 (2014) 57–63.
[40] C. Evans, An Introduction to Crystal Chemistry, Cambridge University Press, Cambridge, 1964.
[41] S.J. Gaffey, Spectral reflectance of carbonate minerals in the visible and near infrared (0.35–2.55 microns): calcite, aragonite, and dolomite, Am. Mineral. 71 (1–2) (1986) 151–162.
[42] J.R. Harris, D. Rogge, R. Hitchcock, O. Ijewliw, D. Wright, Mapping lithology in Canada's Arctic: application of hyperspectral data using the minimum noise fraction transformation and matched filtering, Can. J. Earth Sci. 42 (2005) 2173–2193.
[43] R. Sharpe, G. Cork, Gypsum and anhydrite, in: J.E. Kogel (Ed.), Industrial Minerals & Rocks, 7th ed., Society for Mining, Metallurgy and Exploration Inc., Englewood, CO, USA, 2006.
[44] R.J. Gettens, R.L. Feller, W.T. Chase, Vermilion and cinnabar, Stud. Conserv. 17 (1972) 45–69.
[45] F. Eperjesi, C.W. Fowler, B.J.W. Evans, The effects of coloured light filter overlays on reading rates in age-related macular degeneration, Acta Opthalm. Scand. 82 (2004) 695–700.
[46] A. Cosentino, Identification of pigments by multispectral imaging; a flowchart method, Herit. Sci. 2 (2014) 8.